Air-Stable and Efficient PbSe Quantum-Dot Solar Cells Based upon ZnSe to PbSe Cation-Exchanged Quantum Dots

Sungwoo Kim,[#,†,‡] Ashley R. Marshall,[#,†,§] Daniel M. Kroupa,[†,§] Elisa M. Miller,[†] Joseph M. Luther,[†] Sohee Jeong,[*,‡] and Matthew C. Beard[*,†]

[†]National Renewable Energy Laboratory, Golden, Colorado 80401, United States, [‡]Nanomechanical Systems Research Division, Korea Institute of Machinery and Materials, Daejeon 305-343, Republic of Korea, and [§]Department of Chemistry and Biochemistry, University of Colorado, Boulder, Colorado 80309, United States. [#]These two authors contributed equally to this work.

ABSTRACT We developed a single step, cation-exchange reaction that produces air-stable PbSe quantum dots (QDs) from ZnSe QDs and PbX_2 (X = Cl, Br, or I) precursors. The resulting PbSe QDs are terminated with halide anions and contain residual Zn cations. We characterized the PbSe QDs using UV–vis–NIR absorption, photoluminescence quantum yield spectroscopy, X-ray diffraction, X-ray photoelectron spectroscopy, and transmission electron microscopy. Solar cells fabricated from these PbSe QDs obtained an overall best power conversion efficiency of 6.47% at one sun illumination. The solar cell performance without encapsulation remains unchanged for over 50 days in ambient conditions; and after 50 days, the National Renewable Energy Laboratory certification team certified the device at 5.9%.

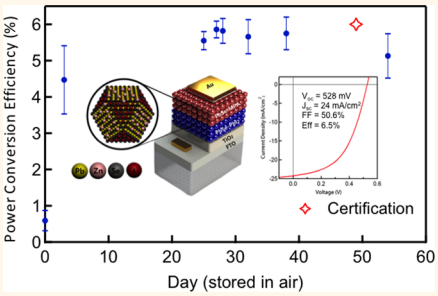

KEYWORDS: quantum dots · cation exchange · halide passivation · PbSe QDs · solar cells

Colloidal quantum dots (QDs) are being investigated because of their beneficial optical and electrical properties, such as band gap tunability, strong absorption over a broad wavelength range, intrinsically large dipole moments, good photostability, and multiple exciton generation (MEG).[1−3] To exploit these desirable properties, researchers are exploring the use of QDs in various applications such as solar cells, light-emitting diodes (LEDs),[4,5] bioimaging,[6] and field effect transistors (FETs).[7] QD-based solar energy conversion strategies are attracting considerable interest because solar energy is renewable, eco-friendly, and sustainable. The main factors that determine the efficiency of QD based solar cells include an optimized solar cell device structure and improved interfacial contact between the QD and charge separating layers. Research efforts have improved the transport characteristics of the *n*-type window layer (*e.g.*, TiO_2, ZnO, or CdS) and *p*-type PbE (E = S or Se) QDs.[8,9] Specifically, PbSe QD solar cells are a focus because of their potential to exceed the Shockley–Queisser limit and approach the Ross–Nozik[10] limit *via* MEG. For example, Semonin *et al.* fabricated a QD solar cell with a peak external quantum efficiency (EQE) of more than 100% using PbSe QDs.[11] However, the performance of PbSe QD-based solar cells tends to quickly degrade upon exposure to air because of oxidation of the photoactive QD layers. Optical shifts observed in steady-state absorption and photoluminescence (PL) suggest that surface oxidation induces important changes in the electronic structure of the QDs related to the reduction in their diameter.[12−14] Improving the stability of QD systems is an important task that should enable a greater degree of reproducibility and uniformity.

Strategies to enhance the optical and electrical properties as well as improve the physical, chemical, and photostability of PbSe QDs have been developed including PbSe/CdSe[15] and PbSe/PbS[16] core/shell structures as well as PbS_xSe_{1-x}[17] alloy structures. Although core/shell structures improve

* Address correspondence to sjeong@kimm.re.kr, matt.beard@nrel.gov.

Received for review April 18, 2015 and accepted July 29, 2015.

Published online July 29, 2015
10.1021/acsnano.5b02326

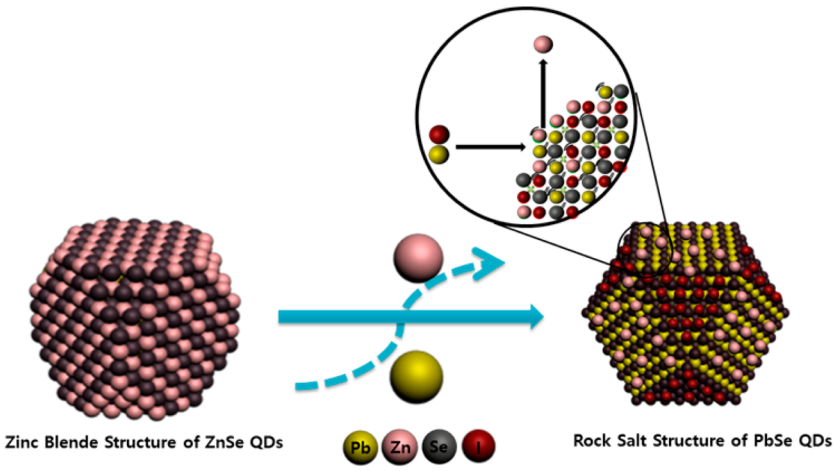

Scheme 1. A Schematic Illustration of the Cation-Exchange Reaction by the Pb-Halide Precursor and ZnSe QDs

the air stability, the electrical transport in films made from core/shell QDs can be impeded by the localization of one or both charge carriers in the core, rendering subsequently fabricated charge separation architectures useless. Therefore, surface treatments that result in stable QDs without impeding charge transport have gained interest in the literature. As a result, several robust methods for improving the stability of QDs *via* surface treatments have been developed. Halide treated PbS QDs have shown promise in improving solar cell[18,19] performance and similar halide terminated PbSe QDs follow similar trends.[22,27] Bae *et al.* improved the air stability of PbSe QDs by employing chlorine gas and hypothesized that a surface passivation layer of $PbCl_x$ forms to protect the PbSe core.[20] Woo *et al.* developed an NH_4X (X = Cl, Br, or I) surface treatment and hypothesized that the improved stability results from the formation of a PbX_2 passivation layer that protects the {100} facets.[21] Zhang *et al.* studied the use of Pb-halide precursors in a direct heat-up synthesis of PbE QDs[22] and found improved air stability of the halide terminated QDs.

Another approach to synthesizing air stable PbSe QDs is through a cation-exchange reaction.[27] Cation-exchange reactions are an increasingly popular approach to synthesizing QDs because morphologically well-defined nanocrystals, prepared by traditional hot injection methods, can be used as an anion template for the preparation of compositionally pure and alloyed nanocrystal structures. Some of these are otherwise inaccessible by direct synthetic methods.[23] Additionally, there is evidence that residual metal ions present during the reaction can effectively passivate deleterious defect states leading to improved performance.[24] Such improvements from metal cations have been explored experimentally[25] and theoretically.[26] We found evidence that improvements in QD solar cell performance are likely a combination of both halide and metal passivation.[27] Accordingly, cadmium and halide treated PbSe QDs have been developed for QD photovoltaics. Zhang *et al.* developed a cation-exchange reaction starting from presynthesized CdSe QDs to produce PbSe QDs and found that PbSe QD solar cells with ~6% power conversion efficiency could be fabricated in ambient conditions. However, those solar cells degraded from 6% to 4% in a few days when stored in air making further improvements necessary. Therefore, we extend the cation-exchange reaction developed by Zhang *et al.*[27] to ZnSe as the starting QD material to synthesize air stable, PbSe QDs.

RESULTS AND DISCUSSION

We developed a direct, cation-exchange procedure that produces PbSe from ZnSe QDs. Presynthesized ZnSe QDs and PbX_2 are the precursors for size-tunable, air-stable PbSe QDs with both halide anion and zinc cation passivation. Detailed experimental procedures and characterization techniques are provided in the methods section. Our cation-exchange reaction is depicted in Scheme 1, which is similar to the methodology reported by Zhang *et al.*[27] First, ZnSe QDs are synthesized following previous reports,[28] using diethyl-zinc (Et_2Zn) and tri-*n*-octylphosphine selenide (TOP-Se) as zinc and selenium precursors. The resulting ZnSe QDs have a first exciton peak at 3.3 eV (Figure 1c) which according to literature reports corresponds to an average diameter of ~3 nm (Figure 1c).[29,30] Supporting Information, Figure S1 shows transmission electron microscopy (TEM) pictographs of the precursor ZnSe QDs and TEM analysis shows an average size of ~3.3 nm (Figure S4) with about a 5% size distribution. To cation-exchange ZnSe QDs to PbSe QDs, PbX_2 precursors are dissolved in oleylamine (OAm) by being heated to 140 °C. ZnSe QDs are dispersed in ODE at room temperature and injected into the PbX_2/OAm complex at injection temperatures ranging from 80 to 200 °C. Finally, oleic acid (OA) is injected into the final solution to both exchange the native OAm ligands and to help remove the QDs from residual PbX_2/OAm.

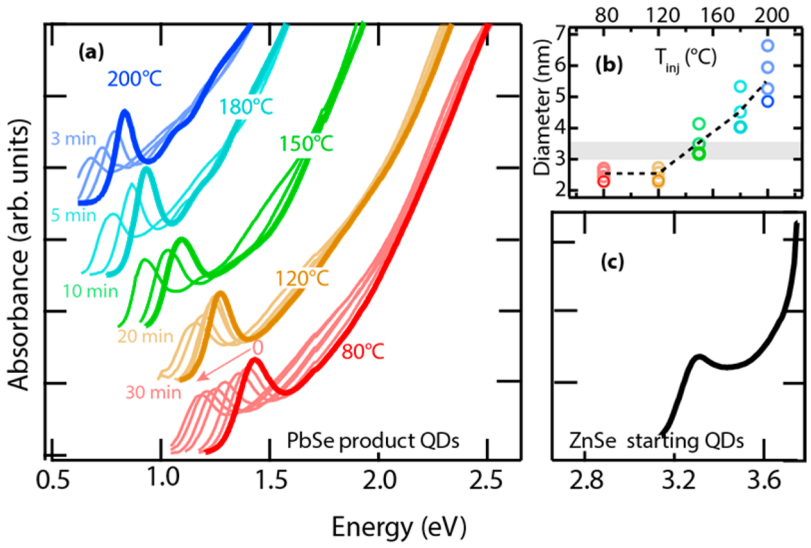

Figure 1. (a) Evolution of absorption spectra of PbSe QDs exchanged from ZnSe in a PbI_2/OAm heterogeneous solution at different injection temperatures. (b) The diameter of the resulting PbSe QD domain as calculated from standard sizing curves. The colored markers correspond with the temperatures used in panel a. The shaded box is the ZnSe QD precursor diameter. (c) Absorption spectrum of precursor ZnSe QDs.

The precursor ZnSe QDs are injected into a vigorously stirred PbX_2/OAm mixture at various injection temperatures. The cation exchange occurs rapidly and can be followed by the appearance of a sharp first exciton peak in the near-IR (Figure 1a, bold traces) and the transformation of the X-ray diffraction (XRD) peaks from those corresponding to ZnSe (Figure S1c, black-trace) to those of PbSe (Figure S1c, red-trace). To collect the spectra displayed in Figure 1a, small aliquots were removed from the reaction vessel, and the UV−vis absorbance was recorded. The first absorption spectra (bold traces) are from aliquots taken immediately (within ∼10 s) after injection of the ZnSe sample, as the reaction proceeds, the PbSe QDs continue to grow (Figure 1a, shaded-traces). The final size of the product PbSe QDs is determined by the injection temperature and reaction time (Figure 1b).

Higher injection temperatures result in both larger initial PbSe QDs and induce a faster subsequent growth phase. These observations suggest that the cation-exchange reaction is thermally activated, similar to other cation-exchange reactions.[32] Such cation-exchange reactions have been described in terms of a temperature-dependent, reaction-zone width.[32] For complete cation exchange with minimal structural distortion, the reaction-zone width should be larger than the precursor QDs. In that case, all of the cations within the QD are in flux (the larger anion sublattice is relatively stable under these conditions). When the reaction-zone width is smaller than the QDs, the reaction occurs within a smaller area of the QD producing a ZnSe/PbSe interface, and complete exchange is achieved by allowing the reaction-zone to propagate through the crystal. When the size of the PbSe QDs is calculated based upon the first exciton peak and standard sizing curves,[31] we find that the product diameter is smaller than the precursor ZnSe diameter when the injection temperature is less than 150−160 °C (Figure 1b shaded box). This suggest that the zone width encompasses the 3.3 nm QDs when the injection temperature is > ∼150 °C. For lower temperatures, complete exchange occurs by allowing the reaction to proceed. Figure S1 panels a and b show TEM images of the precursor ZnSe QDs and the final product PbSe QDs (end reaction times are noted on Figure 1a). At high temperatures, the initial size is apparently already larger than the starting ZnSe QDs. Thus, there is a near-instantaneous cation exchange followed by subsequent growth in a bath of Zn cations. The initial size-distribution decreases for higher injection temperatures because the cation exchange occurs more uniformly. However, higher temperatures induce a faster subsequent growth phase and the size distribution (Figures S3 and S5−S9) increases with increasing time at higher temperatures. Following the procedure developed here, the diameter of the PbSe QDs (Figure 1b) can be tuned over a broad range (∼1.8 nm to ∼7 nm) as determined by standard sizing curves.

For injection temperatures less than 150 °C partial exchange occurs, and there are two possible reaction pathways that are consistent with our results: (1) after partial cation exchange, the PbSe component continues to grow at the interface of the ZnSe/PbSe, analogous to what was observed in the CdS/PbS system[33] and/or (2) the partial cation exchange is accompanied by dissolution of the remaining ZnSe component.[34] We find that the size distribution of the PbSe QDs changes with injection temperature and growth time. The size distribution improves at higher temperatures and larger product sizes for the initially prepared samples.

The XRD patterns and TEM images (Figure 2) suggest a single phase of PbSe particles following injection of ZnSe QDs at 150 °C. Also, the UV−vis spectra do not exhibit high-energy features that could be assigned to residual ZnSe (data not shown). This is in contrast to the partial cation exchange of CdS to PbS results, which do show features of the residual CdS in the TEM, XRD, and UV−vis.[33] These observations suggest that after partial exchange residual ZnSe dissolves producing single phase PbSe QDs. We have not attempted to find reaction conditions that would preserve the partially exchanged nanostructures.

We investigated various Pb-halide precursors as the Pb source for the cation-exchange reaction, including PbF_2, $PbCl_2$, $PbBr_2$, and PbI_2. All of the Pb-halide precursors, except for PbF_2, resulted in successful exchange of ZnSe to PbSe QDs (Figure 1, S10, S11, S12). This is in contrast to the CdSe to PbSe cation-exchange reaction where only $PbCl_2$ was found to induce the cation-exchange reaction. For the various halide precursors, we did not observe large differences in the product PbSe QD size upon the initial injection of ZnSe QDs, since this is a temperature-dependent reaction. The subsequent growth phase, however, did vary with halide precursor. The growth phase was faster and resulted in size defocusing for $PbBr_2$ and PbI_2 compared to $PbCl_2$ (Figure 1, S10 and S11). These observations are consistent with that found in the direct synthesis of PbE QDs from PbX_2/OAm heterogeneous mixtures.[22] In that reaction, PbE QD growth is governed by diffusion of monomers in a viscous heterogeneous reaction bath. The viscosity increases from PbI_2 to $PbCl_2$, which results in faster diffusion in the PbI_2 mixture, causing the growth to approach the reaction-controlled regime and the size-distribution to defocus. Here, the size defocusing regime is reached only when the reaction is allowed to proceed well beyond the initial, cation-exchange step.

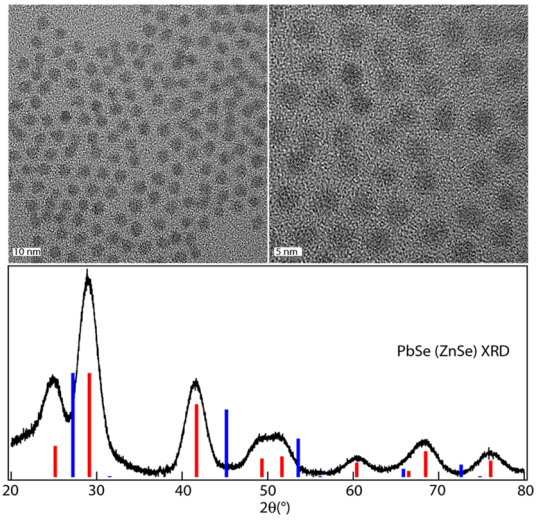

Figure 2. (top) TEM and HR-TEM images of cation exchanged PbSe QDs (scale bar, 10 nm, 5 nm); (bottom) XRD pattern of cation exchanged PbSe QDs. The red lines are the known positions for PbSe and blue lines are the known positions for ZnSe demonstrating that the ZnSe QDs are transformed to PbSe. Standard for Zinc blende ZnSe QDs taken from JCPDS #37-1463 and for rock salt PbSe from JCPDS #06-0354.

In contrast to both the diffusion controlled direct synthesis of PbS and PbSe and the cation exchange from CdSe/CdS, the ZnSe/PbSe system described here enables the direct production of PbSe QDs with Cl, Br, or I termination while retaining good size distributions. We compared the stability of the PbSe QDs when employing various PbX_2 precursors by storing the product QDs in tetrachloroethylene (TCE) under ambient conditions for 50 days and monitoring the absorbance. The degree of blue-shifting of the first exciton feature monitored by UV−vis (Figure 3a) is an indicator of the degree of oxidation, which varies as $PbCl_2$ > $PbBr_2$ > PbI_2. We rationalize this trend by considering the hard and soft Lewis acid and base theory (HSAB). Pb^{2+} is a borderline acid; iodide is a soft base; bromide is a borderline base; and chloride is a hard base. This suggests that iodide and bromide would have improved coordination of surface bound Pb^{2+} ions compared to chloride, which could help explain the increased effectiveness of iodide and bromide at protecting the surface compared to chloride.

We also compared the stability of PbSe QDs synthesized from different formulations by preparing PbSe QDs with a first exciton peak at ~1550 nm from four different reaction protocols: (1) standard PbO synthesis[30] ($PbSe_{PbO}$); (2) PbSe synthesized directly using the $PbCl_2$/OAm diffusion based synthesis[21] ($PbSe_{PbCl_2}$); (3) PbSe

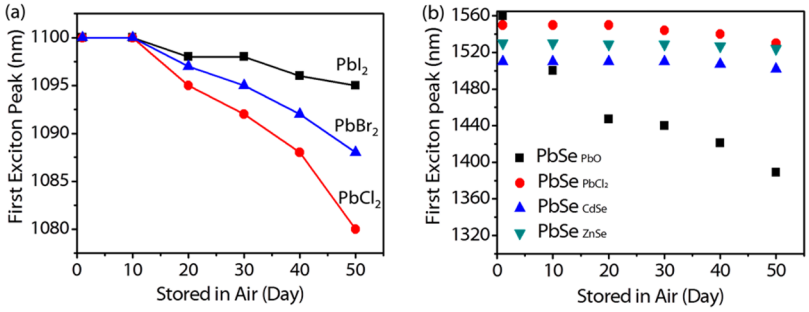

Figure 3. (a) Stability comparison of PbSe QDs cation exchanged from ZnSe using PbX_2 (X = I, Br, or Cl) with an injection temperature at 150 °C. (b) Stability comparison of PbSe QDs synthesized from four reaction protocols.

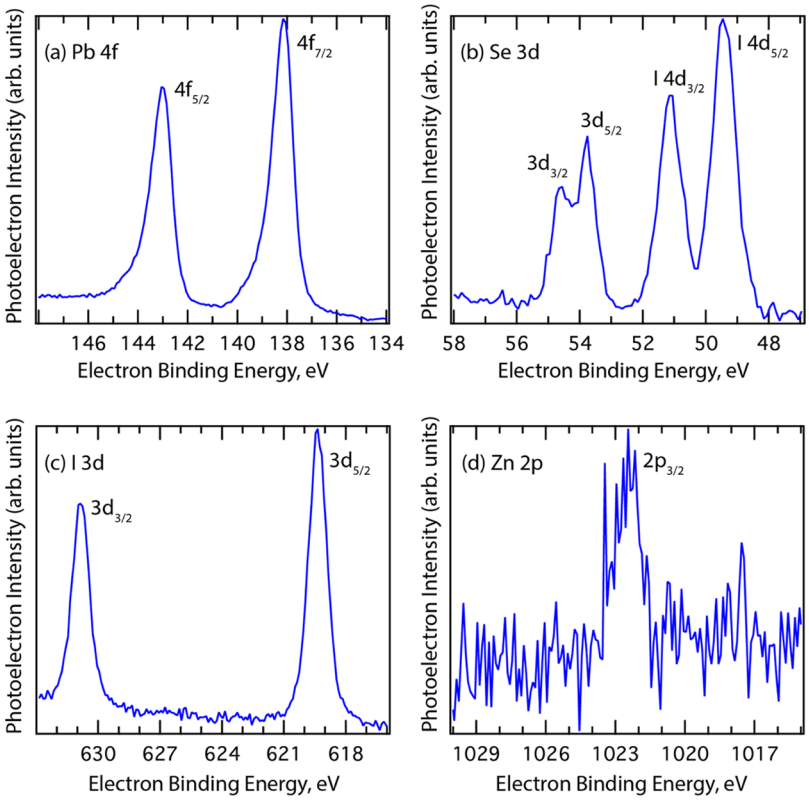

Figure 4. HR-XPS spectra of ZnSe/PbI_2 synthesized PbSe QDs: (a) Pb 4f spectral region; (b) Se 3d spectral region; (c) I 3d spectral region; (d) Zn 2p spectral region.

cation exchanged from CdSe in $PbCl_2$[26] ($PbSe_{CdSe}$); and (4) the cation exchange from ZnSe/PbI_2 presented here ($PbSe_{ZnSe}$) with an injection temperature at 200 °C. We stored the samples in TCE under ambient conditions and compared their absorbance spectra. All of the QDs terminated with a halide show better stability than the PbO synthesized QDs that are terminated only with oleate ligands. While the difference is not large, there does appear to be an advantage to the cation-exchanged QDs that have both halide termination and some residual metal cations (Cd, Zn). We also verified that smaller QDs (Figure S13 for 980 nm) displayed similar stability. In that case, the first exciton peak blue-shifted by 5−10 nm, but the PLQY increased from 22.2 to 27.2% (Figures S13 and S14).

We focused all subsequent experiments on the ZnSe/PbI_2 synthesized PbSe QDs with an injection temperature at 120 °C. The presence of residual zinc and iodide on the PbSe QDs can be confirmed by high-resolution X-ray photoelectron spectroscopy (HR-XPS) (Figure 4). We observe a shift of both the Pb 4f peak and Se 3d peaks to higher binding energies relative to PbO-synthesized QDs suggesting Pb−I terminated QDs.[19] Such shifts are consistent with our study of PbS QDs that had been treated with NH_4I[35] (where no Zn is present) and a study where PbSe QDs had been treated by NH_4Cl.[21] The detection of I and Zn spectral features (Figure 4 panels c and d, respectively) confirms that Zn and I are integrated into the PbSe QD films. For the 2.8 nm diameter PbSe QD film (HR-XPS results shown in Figure 4), we find the ratio of Pb/S to be 2.4, Pb/I to be 3 and Pb/Zn to be 27. We can vary the relative amounts of Pb and I within the QD films (and consequently Pb/O). When QD films are made with a higher Pb/I ratio, we observe a Pb 4f main peak position that is shifted to lower binding energy and loss of the higher energy shoulder (Figure S15). The shift to lower binding energy in Figure S15 strongly suggests a reduced Pb−I environment on the surface, and the loss of the high-energy shoulder could be from a reduced Pb−I environment (and/or Pb−O environment). From the combination of these XPS elemental data and the XRD, it is reasonable to conclude that iodide anions partially terminate the QDs along with oleate ligands. While the precise location of the Zn cations cannot be deduced by the experiments conducted here, it is likely that they also reside near the surface, but at a much lower concentration.

QD solar cells were fabricated from PbSe QDs (963 nm first exciton peak), following a metal halide solid-state fabrication procedure.[19] First, a film of QDs is deposited on the n-type window layer (TiO_2) by dip-coating using PbI_2 in *N,N*-dimethylformamide (DMF) to remove the native oleate ligands. A thinner PbSe QD layer is deposited on the back using mercaptopropionic acid (MPA) in methanol (MeOH). The full device structure (Figure 5a,b) consists of FTO/TiO_2/$PbSe_{PbI_2}$/$PbSe_{MPA}$/Au (details provided in the experimental section). The total thickness of the QD photoactive

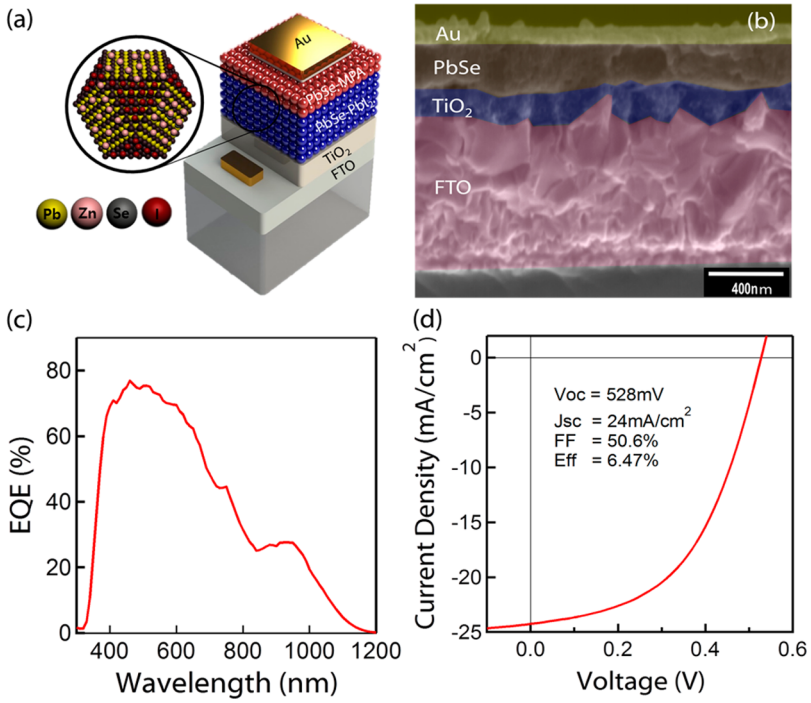

Figure 5. (a) Schematic illustration of the employed device structure. (b) Cross-sectional SEM (scanning electron microscopy) image of a completed device. (c) EQE (external quantum efficiency) spectrum and (d) *J*−*V* curve of the highest efficiency device.

layer is *ca.* 200 nm (Figure 5b, SEM analysis). We hypothesize that the $PbSe_{MPA}$ layer blocks electron flow to the Au anode from the $PbSe_{PbI_2}$ layer, thereby reducing interfacial recombination at the PbSe QD/Au interface. Chuang *et al.* reported a similar approach but used TBAI and ethanedithiol (EDT) ligands to produce a PbS_{TBAI}/PbS_{EDT}[18] bilayer device. Semonin *et al.* also employed two ligands, EDT and hydrazine (Hyd), to produce a PbSe QD bilayer ($PbSe_{EDT}/PbSe_{Hyd}$) device.[3]

The external quantum efficiency (EQE) (Figure 5c) reaches ~30% at the first absorption feature of 980 nm and is close to 80% throughout the visible region. To characterize the device, we measured the photocurrent density−voltage (*J*−*V*) curves (Figure 5d) under AM1.5 illumination in an inert atmosphere. The best cell exhibited a power conversion efficiency (PCE) of 6.47%, with an open circuit voltage (V_{oc}) of 528 mV, a short circuit current density (J_{sc}) of 24 mA/cm^2, and a fill factor (FF) of 50.6%. Similar to Semonin *et al.*, we find that the device efficiency improves after 1−4 days.[3] We stored the solar cell in air without any encapsulation for 55 days, while tracking the device performance (Figure 6) and find that the device performance is stable for over 50 days. After 50 days of storage in air, the cell was certified by the NREL certification team and achieved a 5.9% PCE (Figure S16). This is the first certification of a PbSe based QD solar cell.

We postulate that I ions from the cation-exchange reaction are responsible for the stability exhibited by devices made from the PbSe (ZnSe) QDs. Halide ions greatly improve the air stability of PbSe QDs, rendering the surface resistant to oxidation.[20,22,27] Figure 3b

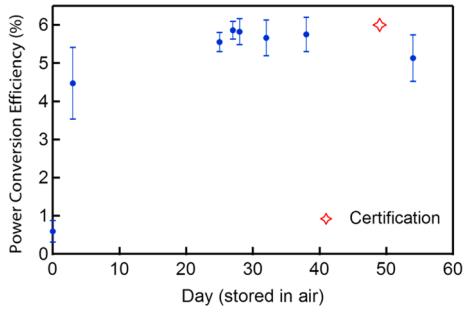

Figure 6. Long-term stability measurement of PbSe (ZnSe) QD device performance, stored in air without encapsulation.

clearly shows that synthetic routes for PbSe QDs utilizing halide precursors result in air-stable QDs, also the XPS data discussed above shows a very low Zn content, while I ions are much more prevalent. Residual iodide ions from the cation-exchange reaction, along with the iodide from the ligand exchange, appear to passivate and protect the PbSe QD surface, so that device fabrication and storage in air does not affect the QD film. Looking at Figure 3b, the $PbSe_{PbCl2}$ QDs show similar air stability to the cation exchanged QDs. Residual Zn^{2+} ions may passivate other surface states, contributing to better device efficiency but do not play a large role in improving the air stability.

CONCLUSIONS

We developed and synthesized size tunable PbSe QDs *via* a single-step, cation-exchange reaction from ZnSe QDs and Pb-halide precursors. We find improved PbSe QD air stability with iodide passivated QDs

exhibiting better solution air stability than other halide (bromide or chloride) ions. Improving the air stability of cation-exchanged PbSe QDs enables us to fabricate solar cell devices that can utilize more of the solar spectrum, specifically the NIR. We fabricated devices using a TiO_2/QD heterojunction and obtained a laboratory best PCE of 6.47%. Furthermore, the device performance without encapsulation remains unchanged (standard deviation ~5%) for over 50 days under ambient conditions.

MATERIALS AND EXPERIMENTAL METHODS

Materials. Lead iodide (PbI_2), lead chloride ($PbCl_2$), lead bromide ($PbBr_2$) (99.999%), oleylamine (OAm, tech. grade, 70%), oleic acid (OA, tech. grade, 90%), diethyl-zinc (Et_2Zn, 0.5 M in toluene), 1-octadencene (ODE, tech. grade, 90%), selenium powder (99.99%), tri-*n*-octylphosphine (TOP, tech. grade, 90%), trioctylphosphine oxide (TOPO, tech. grade, 90%), 3-mercaptopoprionic acid (MPA, > 99%), tetrachloroethylene (TCE, > 99.9%), hexadecylamine (HDA, > 90%), *N*,*N*-dimethylformamide (DMF, anhydrous, 99.8%), hexane (95%), and ethanol (>99.5%) were purchased from Aldrich.

Synthesis of ZnSe QDs. ZnSe QDs were synthesized using the methodology reported by Kim *et al.*[28]

For a typical reaction, HDA (1449 mg, 6 mmol) and TOPO (9.3 g, 24 mmol) were heated to 125 °C and degassed under vacuum for 2 h in a three neck flask. Then, the solution was heated to 320 °C under N_2 atmosphere. To make the injection solution, Et_2Zn (1.2 mmol) and 1.2 mL of 1 M TOP−Se stock solution were mixed in 3 mL of TOP in a glovebox. The injection solution was rapidly added to the three-neck flask at 320 °C. The solution was maintained at 270 °C for 1 h then cooled to room temperature. The resulting ZnSe QDs were isolated by precipitation with ethanol and subsequently redispersed into ODE.

Synthesis of PbSe QD *via* Cation Exchange. The cation-exchanged PbSe QDs were synthesized using a modified procedure similar to that reported in Zhang *et al.*[27]

OAm (10 mL) and PbI_2 (1.2 mmol) were heated to 140 °C and kept under vacuum for 1 h to degas and remove water. The mixture was then cooled to the desired reaction temperature. An injection of ZnSe QDs (80 mg) in ODE was added under N_2. The reaction mixture was kept at temperature for 3−30 min and then cooled to 40 °C. An 8 mL of aliquot of OA was added to the reaction solution and stirred for 20 min. The QDs were washed twice by precipitating with 40 mL of ethanol, centrifuged to remove the solids, and then redissolved in hexane.

first exciton position (nm)	injection temperature (°C)	final growth time (min)
850−1050	80	30
940−1180	120	20
980−1370	150	10
1250−1580	180	5
1420−1880	200	3

Characterization. Absorption spectra were measured by a Shimadzu UV−vis−NIR 3600 spectrophotometer. The PL QY data were obtained using a LabSphere integrating sphere with excitation provided monochromatic light. TEM images and HR-TEM were taken on a FEI Tecnai G2 20-Twin electron microscope with an accelerating voltage of 200 kV. Carbon-coated copper grids were dipped in QD hexane solutions. HP-XRD patterns were obtained using a Bruker D8 Discover diffractometer using Cu Kα radiation. XPS results were obtained using the Physical Electronics 5600 photoemission system using Al Kα radiation. A more detailed discussion can be found in ref 36. Briefly, the XPS spectra were calibrated using known metallic transitions, and all samples shown here did not exhibit photocharging.

Solar cell devices were measured under AM1.5 illumination in an inert atmosphere using a Newport solar simulator calibrated with a Si photodiode (Hamamtsu, S1787−04). An aperture of 0.06 cm^2 was used when measuring JV curves, the full device area is 0.101 cm^2. External quantum efficiency measurements were also performed under inert atmosphere on an Oriel IQE-200 system.

PL QY Measurements. PL QY measurements were made using a previously established method.[1] QDs were dispersed in TCE with an absorbance of less than 0.1 OD to minimize reabsorption effects. The measurements were taken in a LabSphere integration sphere with an 850 nm NIR-LED (ThorLabs M850L3) excitation source passed through an 850 nm centered 40 nm band-pass filter. Light from the sphere was fiber coupled to a home-built fluorescence spectrometer consisting of a monochromator (PTI) and a two-stage thermocouple-cooled extended InGaAs detector. The excitation LED was driven by a 15 V square wave at 25 Hz using a Stanford Research Systems (SRS) DS335 function generator. The detector signal was amplified using a SRS SR530 lock-in amplifier, and all spectra were corrected for grating, fiber, integration sphere, and detector deficiencies using a calibrated lamp.

The PL QY was calculated using

$$\mathrm{PLQY} = \frac{\int I_{\mathrm{sample}}(\lambda) - I_{\mathrm{ref}}(\lambda)\,\mathrm{d}\lambda}{\int E_{\mathrm{ref}}(\lambda) - E_{\mathrm{sample}}(\lambda)\,\mathrm{d}\lambda}$$

where *I* indicates the measured intensity of the emitted light, *E* indicates the measured intensity of the excitation light, "sample" indicates measurements of QD samples, and 'ref' indicates measurements of a reference cuvette (contains pure solvent, TCE, without QDs).

Device Fabrication. Patterned FTO substrates were purchased from Thin Film Devices. The substrates were rubbed vigorously with ethanol and UV-ozone treated for 5 min before use. TiO_2 sol−gel was prepared by stirring 5 mL of anhydrous ethanol, 2 drops of HCl, 175 μL of deionized water and 375 μL of titanium ethoxide for 48 h under N_2. The TiO_2 sol−gel (70 μL) was spin-coated at 1500 rpm for 30 s. The film was annealed for 30 min at 115 °C on a hot plate, then at 450 °C in an oven. The TiO_2 film was stored in air overnight before use. The PbSe QD film was deposited by dip-coating with PbSe QDs in hexane (~15 mg/mL) and 10 mM PbI_2 in DMF. QDs were deposited by removing the film quickly, but smoothly from the hexane solution, then soaking in the DMF solution for at least 30 s to fully exchange the film. Excess DMF was rinsed off using acetonitrile, and the film was dried using a stream of air before the next layer was deposited. Sixteen layers of PbSe QDs were deposited using PbI_2, and then two layers were deposited using 10% MPA in methanol (MeOH), with a MeOH rinse to remove excess MPA. A 100 nm sample of gold was deposited by thermal evaporation as the back contact. Devices were stored in air.

Conflict of Interest: The authors declare no competing financial interest.

Supporting Information Available: Additional TEM images and XRD data, detailed temporal evolution of absorption spectra of various PbX_2 (Br or Cl) passivated PbSe QDs samples at different injection temperatures, XPS chemical ratios and additional Pb 4f spectra, PLQY, and device results certified by NREL after 50 days of storage in air. The Supporting Information is available free of charge on the ACS Publications website at DOI: 10.1021/acsnano.5b02326.

(PDF)

Acknowledgment. S.K. was supported at NREL by the Global Frontier R&D program by the Center for Multiscale Energy Systems (2011-0031566) and the Global R&D program (1415134409)

funded by KIAT. The Center for Advanced Solar Photophysics, an Energy Frontier Research Center funded by the Department of Energy, Office of Science, Office of Basic Energy Sciences supported device fabrication. The solar photochemistry program within the Office of Science, Office of Basic Energy Sciences supported synthesis and QD characterization. XPS work was funded by a NREL director's postdoctoral fellowship. DOE funding to NREL was provided through contract DE-AC36-08G028308.

REFERENCES AND NOTES

1. Nozik, A. J.; Beard, M. C.; Luther, J. M.; Law, M.; Ellingson, R. J.; Johnson, J. C. Semiconductor Quantum Dots and Quantum Dot Arrays and Applications of Multiple Exciton Generation to Third-Generation Photovoltaic Solar Cells. *Chem. Rev.* **2010**, *110*, 6873.
2. Schaller, R.; Klimov, V. High Efficiency Carrier Multiplication in PbSe Nanocrystals: Implications for Solar Energy Conversion. *Phys. Rev. Lett.* **2004**, *92*, 186601.
3. Semonin, O. E.; Luther, J. M.; Beard, M. C. Quantum Dots for Nextgeneration Photovoltaics. *Mater. Today* **2012**, *15*, 508–515.
4. Coe, S.; Woo, W.-K.; Bawendi, M. G.; Bulovic, V. Electroluminescence from Single Monolayers of Nanocrystals in Molecular Organic Devices. *Nature* **2002**, *420*, 800–803.
5. Kim, S.; Kim, T.; Kang, M.; Kwak, S. K.; Yoo, T. W.; Park, L. S.; Yang, I.; Hwang, S.; Lee, J. E.; Kim, S. K.; et al. Highly Luminescent InP/GaP/ZnS Nanocrystals and Their Application to White Light-Emitting Diodes. *J. Am. Chem. Soc.* **2012**, *134*, 3804–3809.
6. Bharali, D. J.; Lucey, D. W.; Jayakumar, H.; Pudavar, H. E.; Prasad, P. N. Folate-Receptor-Mediated Delivery of InP Quantum Dots for Bioimaging Using Confocal and Two-Photon Microscopy. *J. Am. Chem. Soc.* **2005**, *127*, 11364–11371.
7. Talapin, D. V.; Murray, C. B. PbSe Nanocrystal Solids for n- and p- Channel Thin Film Field-Effect Transistors. *Science* **2005**, *310*, 86–89.
8. Pattantyus-Abraham, A. G.; Kramer, I. J.; Barkhouse, A. R.; Wang, X.; Konstantatos, G.; Debnath, R.; Levina, L.; Raabe, I.; Nazeeruddin, M. K.; Grätzel, M.; Sargent, E. H. Depleted-Heterojunction Colloidal Quantum Dot Solar Cells. *ACS Nano* **2010**, *4*, 3374–3380.
9. Kamat, P. V. Quantum Dot Solar Cells. Semiconductor Nanocrystals as Light Harvesters. *J. Phys. Chem. C* **2008**, *112*, 18737–18735.
10. Ross, R. T.; Nozik, A. J. Efficiency of Hot-Carrier Solar Energy Converters. *J. Appl. Phys.* **1982**, *53*, 3813.
11. Semonin, O. E.; Luther, J. M.; Choi, S.; Chen, H.-Y.; Gao, J.; Nozik, A. J.; Beard, M. C. Peak External Photocurrent Quantum Efficiency Exceeding 100% *via* MEG in a Quantum Dot Solar Cell. *Science* **2011**, *334*, 1530–1533.
12. Luther, J. M.; Law, M.; Song, Q.; Perkins, C. L.; Beard, M. C.; Nozik, A. J. Structural, Optical and Electrical Properties of Self-Assembled Films of PbSe Nonocrystals Treated with 1,2-Ethanedithiol. *ACS Nano* **2008**, *2*, 271–280.
13. Peterson, J. J.; Krauss, T. D. Photobrightening and Photodarkening in PbS Quantum Dots. *Phys. Chem. Chem. Phys.* **2006**, *8*, 3851–3856.
14. Stouwdam, J. W.; Shan, J.; Van Veggel, F. C. J. M.; Pattantyus-Abraham, A. G.; Young, J. F.; Raudsepp, M. Photostability of Colloidal PbSe and PbSe/PbS Core/Shell Nanocrystals in Solution and in the Solid State. *J. Phys. Chem. C* **2007**, *111*, 1086–1092.
15. Zhang, Y.; Dai, Q.; Li, X.; Liang, J.; Colvin, V. L.; Wang, Y.; Yu, W. PbSe/CdSe and PbSe/CdSe/ZnSe Hierarchical Nanocrystals and Their Photoluminescence. *Langmuir* **2011**, *27*, 9583–9587.
16. Yanover, D.; Capek, R. K.; Brusilovski, A. R.; Vaxenburg, R.; Grumbach, N.; Maikov, G. I.; Solomeshch, O.; Sashchiuk, A.; Lifshitz, E. Small-Sized PbSe/PbS Core/shell Colloidal Quantum Dots. *Chem. Mater.* **2012**, *24*, 4417–4423.
17. Nam, M.; Kim, S.; Kim, S.; Kim, S.-W.; Lee, K. Efficent Hybrid Solar Cells Using PbS_xSe_{1-x} Quantum Dots and Nanorods for Broad-Range Photon Absorption and Well-Aseembled Charge Transfer Networks. *Nanoscale* **2013**, *5*, 8202–8209.
18. Chuang, C.-H. M.; Brown, P. R.; Bulovic, V.; Bawendi, M. G. Improved Performance and Stability in Quantum Dot Solar Cells Through Band Alignment Engineering. *Nat. Mater.* **2014**, *13*, 796–801.
19. Crisp, R. W.; Kroupa, D. M.; Marshall, A. R.; Miller, E. M.; Zhang, J.; Beard, M. C.; Luther, J. M. Metal Halide Solid-State Sirface Treatment For High Efficiency PbS and PbSe QD Solar Cells. *Sci. Rep.* **2015**, *5*, 9945–9950.
20. Bae, W. K.; Joo, J.; Padilha, L. A.; Won, J.; Lee, D. C.; Lin, Q.; Koh, W.; Luo, H.; Klimov, V. I.; Pietryga, J. M. Highly Effective Surface Passivation of PbSe Quantum Dots through Reaction with Molecular Chlorine. *J. Am. Chem. Soc.* **2012**, *134*, 20160–20168.
21. Woo, J. Y.; Ko, J.-H.; Song, J. H.; Kim, K.; Choi, H.; Kim, Y. H.; Lee, D. C.; Jeong, S. Ultrastable PbSe Nanocrystal Quantum Dots *via in Situ* Formation of Atomically Thin Halide Adlayers on PbSe (100). *J. Am. Chem. Soc.* **2014**, *136*, 8883–8886.
22. Zhang, J.; Gao, J.; Miller, E. M.; Luther, J. M.; Beard, M. C. Diffusion-Controlled Synthesis of PbS and PbSe Quantum Dots with *in Situ* Halide Passivation for Quantum Dot Solar Cells. *ACS Nano* **2014**, *8*, 614–622.
23. Fayette, M.; Robinson, R. D. Chemical Transformations of Nanomaterials for Energy Applications. *J. Mater. Chem. A* **2014**, *2*, 5965–5978.
24. Spanhel, L.; Haase, M.; Weller, H.; Henglein, A. Photochemistry of Colloidal Semiconductors. 20. Surface Modification and Stability of Strong Luminescing CdS Particles. *J. Am. Chem. Soc.* **1987**, *109*, 5649–5655.
25. Ip, A. H.; Thon, S. M.; Hoogland, S.; Voznyy, O.; Zhitomirsky, D.; Debnath, R.; Levina, L.; Rollny, L. R.; Carey, G. H.; Fischer, A.; et al. Hybrid Passivated Colloidal Quantum Dot Solids. *Nat. Nanotechnol.* **2012**, *7*, 577–582.
26. Voznyy, O.; Thon, S. M.; Ip, A. H.; Sargent, E. H. Dynamic Trap Formation and Elimination in Colloidal Quantum Dots. *J. Phys. Chem. Lett.* **2013**, *4*, 987–992.
27. Zhang, J.; Gao, J.; Church, C. P.; Miller, E. M.; Luther, J. M.; Klimov, V. I.; Beard, M. C. PbSe Quantum Dot Solar Cells with More than 6% Efficiency Fabricated in Ambient Atmosphere. *Nano Lett.* **2014**, *14*, 6010–6015.
28. Kim, S.; Park, J.; Kim, T.; Jang, E.; Jun, S.; Jang, H.; Kim, B.; Kim, S.-W. Reverse Type-I ZnSe/InP/ZnS Core/Shell/Shell Nanocrystals: Cadmium- Free Quantum Dots for Visible Luminescence. *Small* **2011**, *7*, 70–73.
29. Hines, M. A.; Guyot-Sionnest, P. Bright UV-Blue Luminescent Colloidal ZnSe Nanocrystals. *J. Phys. Chem. B* **1998**, *102*, 3655–3657.
30. Nikesh, V. V.; Lad, A. D.; Kimura, S.; Nozaki, S.; Mahamuni, S. Electron Energy Levels in ZnSe Quantum Dots. *J. Appl. Phys.* **2006**, *100*, 113520.
31. Smith, D. K.; Luther, J. M.; Semonin, O. E.; Nozik, A. J.; Beard, M. C. Tuning the Synthesis of Ternary Lead Chalcogenide Quantum Dots by Balancing Precursor Reactivity. *ACS Nano* **2011**, *5*, 183–190.
32. Son, D. H.; Hughes, S. M.; Yin, Y.; Alivisatos, A. P. Cation Exchange Reactions in Ionic Nanocrystals. *Science* **2004**, *306*, 1009–1012.
33. Zhang, J.; Crisp, R. W.; Kroupa, D. M.; Luther, J. M.; Miller, E. M.; Gao, J.; Beard, M. C. Preparation of Cd/Pb Chalcogenide Heterostructured Janus Particles via Controllable Cation Exchange. *ACS Nano* **2015**, *9*, 7151–7163.
34. Lee, S.; Lee, D. T.; Ko, J.-H.; Kim, W.-J.; Joo, J.; Jeong, S.; McGuire, J. A.; Kim, Y.-H.; Lee, D. C. Slow Colloidal Growth of PbSe Nanocrystals for Facile Morphology and Size Control. *RSC Adv.* **2014**, *4*, 9842–9850.
35. Kim, S.; Noh, J.; Choi, H.; Ha, H.; Song, J. H.; Shim, H. C.; Jang, J.; Beard, M. C.; Jeong, S. One-Step Deposition of Photovoltaic Layers Using Iodide Terminated PbS Quantum Dots. *J. Phys. Chem. Lett.* **2014**, *5*, 4002–2007.
36. Perkins, C. L.; Hasoon, F. S. Surfactant-Assisted Growth of CdS Thin Films for Photovoltaic Applications. *J. Vac. Sci. Technol., A* **2006**, *24*, 497–504.
37. Semonin, O. E.; Johnson, J. C.; Luther, J. M.; Midgett, A. G.; Nozik, A. J.; Beard, M. C. Absolute Photoluminescene Quantum Yields of IR-26 Dye, PbS, and PbSe Quantum Dots. *J. Phys. Chem. Lett.* **2010**, *1*, 2445–2450.